

Particle filtering for passive fathometer tracking

Zoi-Heleni Michalopoulou

Department of Mathematical Sciences, New Jersey Institute of Technology, Newark, New Jersey 07102
michalop@njit.edu

Caglar Yardim and Peter Gerstoft

Marine Physical Laboratory, Scripps Institution of Oceanography, La Jolla, California 92093-0238
cyardim@ucsd.edu, gerstoft@ucsd.edu

Abstract: Seabed interface depths and fathometer amplitudes are tracked for an unknown and changing number of sub-bottom reflectors. This is achieved by incorporating conventional and adaptive fathometer processors into sequential Monte Carlo methods for a moving vertical line array. Sediment layering information and time-varying fathometer response amplitudes are tracked by using a multiple model particle filter with an uncertain number of reflectors. Results are compared to a classical particle filter where the number of reflectors is considered to be known. Reflector tracking is demonstrated for both conventional and adaptive processing applied to the drifting array data from the Boundary 2003 experiment. The layering information is successfully tracked by the multiple model particle filter even for noisy fathometer outputs.

© 2012 Acoustical Society of America

PACS numbers: 43.60.Hj, 43.60.Jn, 43.30.Pc [JC]

Date Received: October 3, 2011 Date Accepted: November 23, 2011

1. Introduction

Extracting information about ocean environment using ambient noise is first demonstrated in Refs. 1 and 2. Passive fathometer data processing³⁻⁶ enables ocean bottom profiling using only the ocean ambient noise that is generated by wave breaking. The fathometer output is the cross-correlation of this downward traveling sea surface noise with the reflection of itself from the seabed. This requires a coherent processing technique such as beamforming on the vertical line array (VLA) recording the noise. Beamforming allows the array to look up and down while rejecting the signals from other angles. Recently, adaptive beamforming such as minimum variance distortionless response (MVDR) beamforming⁶ is used to improve the fathometer results. The fathometer output gives strong correlation of upward and downward traveling noise at certain time delays corresponding to reflections from sediment interfaces. The amplitudes of the peaks also relate to geoacoustic parameters.⁷

The acoustic pressure \mathbf{p} and the steering vectors \mathbf{w} across the array elements are used to compute the upward and downward traveling noise for conventional beamforming. At frequency f , the steering vector entry for the m th array element ($m=0$ for the deepest hydrophone⁸) is $w_m = \exp(imk_f d \sin \theta)$, where d is the array element separation distance, $k_f = 2\pi f/c$ is the wavenumber, c is the sound speed, and θ is the steering angle where $\theta = 90^\circ$ is upward looking.

To observe the noise generated from the sea surface above the array, $\theta = 90^\circ$ is needed. Similarly, observing the noise reflecting from the sea bottom requires $\theta = -90^\circ$. This results in upward and downward looking steering vectors \mathbf{w}_\uparrow and \mathbf{w}_\downarrow , with $\mathbf{w}_\uparrow = \mathbf{w}_\downarrow^*$, where $*$ denotes complex conjugate. Therefore, the upward \mathbf{n}_u and downward \mathbf{n}_d traveling noise across the array will be

$$\mathbf{n}_u = \mathbf{w}_\downarrow^H \mathbf{p} \quad \text{and} \quad \mathbf{n}_d = \mathbf{w}_\uparrow^H \mathbf{p} = \mathbf{w}_\downarrow^T \mathbf{p}, \quad (1)$$

where superscripts H and T represent the complex conjugate transpose and transpose, respectively. Arbitrarily defining $\mathbf{w} = \mathbf{w}_\downarrow$, the correlation between the two noise terms is

$$\mathbf{C}_{conv}(f) = \mathbf{n}_d \mathbf{n}_u^H = (\mathbf{w}^T \mathbf{p})(\mathbf{w}^H \mathbf{p})^H = \mathbf{w}^T \mathbf{R} \mathbf{w}, \quad (2)$$

using conventional beamforming, where $\mathbf{R} = \mathbf{p} \mathbf{p}^H$ is the data cross spectral density matrix. Note that the result is slightly different from the one of a conventional beamformer output due to the transpose instead of the complex conjugate in the first term.

The noise coming from broadside angles is typically much stronger than that from end-fire directions.^{5,6} Thus adaptive beamforming can improve the fathometer results by suppressing the noise from unwanted directions. The MVDR fathometer is shown to perform significantly better than the conventional fathometer.⁶ The MVDR weights $\tilde{\mathbf{w}}$ relate to \mathbf{w} as

$$\tilde{\mathbf{w}}_\downarrow = \frac{\mathbf{R}^{-1} \mathbf{w}_\downarrow}{\mathbf{w}_\downarrow^H \mathbf{R}^{-1} \mathbf{w}_\downarrow} \quad \text{and} \quad \tilde{\mathbf{w}}_\uparrow = \frac{\mathbf{R}^{-1} \mathbf{w}_\uparrow}{\mathbf{w}_\uparrow^H \mathbf{R}^{-1} \mathbf{w}_\uparrow}, \quad \text{with} \quad \tilde{\mathbf{w}}_\downarrow \neq \tilde{\mathbf{w}}_\uparrow^*. \quad (3)$$

The correlation between the upward and downward adaptively beamformed noise gives

$$\mathbf{C}_{mvd}(f) = \mathbf{w}_\downarrow^H \mathbf{R} \mathbf{w}_\uparrow. \quad (4)$$

The time domain fathometer response is given by computing Eqs. (2) and (4) for the frequencies inside the desired bandwidth and then calculating an inverse Fourier transform.

2. Passive fathometer particle filtering

Sequential Bayesian methods enable tracking in dynamic, non-stationary ocean environments. These include both the Kalman family of filters and sequential Monte Carlo methods known as particle filters (PF).^{9,10} The PF gets its name from particles $\{\mathbf{x}_t^i\}_{i=1}^{N_p} = \{\mathbf{x}_t^1, \dots, \mathbf{x}_t^{N_p}\}$, each \mathbf{x}_t representing a possible solution for the tracked parameters. Each possible solution has a weight proportional to its likelihood $\mathcal{L}(\mathbf{x}_t)$, computed using the current data \mathbf{y}_t . The filter estimates both the time-varying (or space-varying) parameters and the evolving uncertainty in these estimates by tracking the posterior probability density function (PDF) $p(\mathbf{x}_t | \mathbf{y}_1 \dots \mathbf{y}_t)$.

Sequential Bayesian methods have been previously used in geoacoustic inversion and relevant applications.^{11–16} Passive fathometer tracking was one of the first suggested geoacoustic applications.¹⁷ The classical PF assumes a fixed model and tracks the associated parameters. However, in many applications, there can be multiple models, each with unknown and different parameters. This requires a multiple model particle filter (MMPF).¹⁸ This filter includes an extra parameter in the state vector that denotes which model each particle uses. The filter not only tracks the model parameters but also the most suitable model itself. Multiple model estimation has been applied to spatial arrival time tracking^{10,19} and multilayer geoacoustic tracking.¹⁴ The spatial arrival time tracking approach, which forms the basis for this work, implements filtering based on importance sampling and tracks both amplitudes and arrival times, also integrating a model transition matrix. The multilayer geoacoustic tracking technique implements a trans-dimensional inversion via reversible-jump Markov-chain Monte Carlo.

When comparing data and observations via the likelihood function, higher-order models (more reflectors) will generally be favored as they provide a better fit to the data. To balance this, higher order models are penalized by incorporating factor $1/N^{m_t}$ as part of the prior PDF, where N is the length of the data vector and m_t is the number of interfaces; this is the foundation of the Bayes Information Criterion. The

prior distribution allows the best match with the smallest model order to be selected.²⁰ The other part of the prior stems from the previous estimate and the state equation, which are discussed in the following text.

The state and measurement equations for fathometer tracking are given as:

$$\mathbf{x}_t = \mathbf{x}_{t-1} + \mathbf{v}_t \tag{5}$$

$$\mathbf{y}_t = \mathbf{h}(\mathbf{x}_t) + \mathbf{w}_t, \tag{6}$$

where \mathbf{v}_t and \mathbf{w}_t are state and measurement noise and $\mathbf{h}(\cdot)$ is the fathometer (either conventional or MVDR) processor. For the PF, the state vector is composed of the reflector depths z and the fathometer output amplitudes a at each of these boundaries for the selected number of reflectors, giving $\mathbf{x}_t = [\mathbf{z}_t^T \ \mathbf{a}_t^T]^T$. For the MMPF, model parameter m_t is also included with $\mathbf{x}_t = [m_t \ \mathbf{z}_t^T \ \mathbf{a}_t^T]^T$. The lengths of vectors \mathbf{z}_t and \mathbf{a}_t are determined by m_t .

The MMPF is based on sequential importance resampling (SIR).¹⁸ For expedience, amplitudes \mathbf{a}_t are computed with the help of marginalization;^{21,22} that is, our MMPF implementation calculates \mathbf{a}_t at each step using maximum likelihood estimation.

The SIR has three stages at each step t :

- (1) Predict: Starting with the particle set from the previous step $\{\mathbf{x}_{t-1}^i\}_{i=1}^{N_p}$, a new set of predictions $\{\mathbf{x}_t^i\}_{i=1}^{N_p}$ is created for t by sampling from the transitional density $p(\mathbf{x}_t|\mathbf{x}_{t-1})$. This is done by propagating each \mathbf{x}_{t-1}^i through the state equation [Eq. (5)] together with a random realization from \mathbf{v}_t .
- (2) Update: Compute the normalized weight of each particle via $w_t^i = \mathcal{L}(\mathbf{x}_t^i) / \sum_{j=1}^{N_p} \mathcal{L}(\mathbf{x}_t^j)$ using Eq. (6) and \mathbf{y}_t .
The set of particles and their weights $\{\mathbf{x}_t^i, w_t^i\}_{i=1}^{N_p}$ represent the posterior density. Quantities such as maximum *a posteriori* (MAP) estimates, mean, variance, or marginal PDFs can be computed using the posterior given by

$$p(\mathbf{x}_t|\mathbf{y}_1 \dots \mathbf{y}_t) \approx \sum_{i=1}^{N_p} w_t^i \delta(\mathbf{x}_t - \mathbf{x}_t^i). \tag{7}$$

- (3) Resample: A resampling stage is needed to keep numerical stability in SIR. This stage redistributes samples, so that the number of samples in a region of state space is proportional to the posterior density of that region. This creates a larger number of samples from high likelihood regions. More details can be found in Refs. 18, 9, and 10.

For the MMPF,^{10,23} a model transition matrix Π_m is needed. The entries of Π_m give the probabilities of particles belonging to a given model to switch to another model. Therefore, an MMPF SIR has an extra model transitioning step before the ‘‘Predict’’ stage. A typical MMPF step involves:

- (1) Model transitioning: Again, start with $\{\mathbf{x}_{t-1}^i\}_{i=1}^{N_p}$, where particle i follows model m_{t-1}^i . Predict the models of new particles m_t^i at t using the model transition matrix. This implies that some state variables \mathbf{x}_k can exit or more state variables can be ‘‘born,’’ with the model order decreasing or increasing, respectively. The dimension of the state vector is, thus, appropriately modified.
- (2) Model conditioned-SIR: Using the newly predicted model m_t^i for each particle, run a model conditioned-SIR exactly as given in the preceding text. Penalization via the prior weighs model orders appropriately.

3. Passive fathometer tracking on Boundary 2003 drifting array data

The ambient noise used in this paper is collected by the drifting array in the NURC Boundary 2003 experiment. The array consists of 32 hydrophones with 0.18 m spacing.

The array drifts at 70–80 m depth with an average reference hydrophone depth of 73.5 m. Frequency bandwidths of 200–4000 Hz and 50–4000 Hz are used for conventional and MVDR fathometers, respectively with a sampling frequency of 12 kHz.⁶ The lower usable frequency in the conventional processor is limited due to the broadside shipping noise at frequencies below 200 Hz. The MVDR has much better side-lobe suppression and, hence, the side-lobe leakage can be tolerated at frequencies as low as 50 Hz. For both cases, 1.4 s snapshots with a total averaging time of 90 s are used. The conventional fathometer results are given in Ref. 3 and the adaptive beamforming results using both MVDR and white noise constraint fathometers are given in Ref. 6.

MMPF results for conventional and MVDR tracking are shown in Fig. 1; 20 000 particles were used. For both cases, the order (number of reflectors) is allowed to vary. It was assumed that seven, eight, or nine reflectors were present. The transition matrix determining probabilities of switching (or not) from one number of reflectors to another was:

$$\Pi_m = \begin{pmatrix} 0.6 & 0.2 & 0.2 \\ 0.2 & 0.6 & 0.2 \\ 0.2 & 0.2 & 0.6 \end{pmatrix}, \tag{8}$$

Figures 1(a) and 1(b) illustrate the fathometer results after the conventional and MVDR processing, respectively. Figures 1(c) and 1(d) show the same results but now with the MAP estimates for the MMPF reflector tracks superimposed (dots). It is observed that the improved resolution of the MVDR facilitates the accurate detection

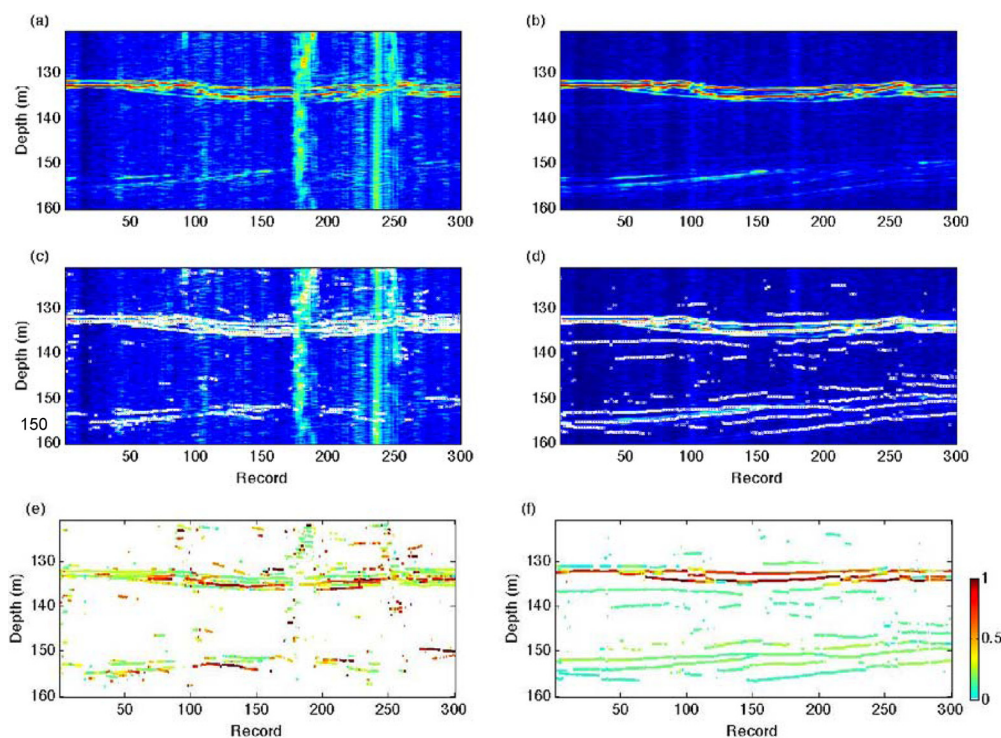


Fig. 1. (Color online) (a) Conventional and (b) MVDR fathometer results for Boundary 2003 data. (c) Conventional and (d) MVDR fathometer results for Boundary 2003 data with MMPF MAP tracks superimposed (dots). MAP estimates of tracked amplitudes for (e) conventional and (f) MVDR fathometer results.

and tracking of reflectors. The conventional processor may miss reflectors, instead identifying isolated noise peaks as reflectors. It is worth noting that the PF becomes more “distracted” by the broadband shipping noise in the conventional case than in the MVDR case, especially around record 180. Figures 1(e) and 1(f) show the track results of fathometer amplitudes at all the reflectors for conventional and MVDR processing, respectively. The amplitudes of reflections near 130 m are large as expected, followed by those close to 155 m which are less pronounced as confirmed by Figs. 1(a) and 1(b).

Figure 2(a) illustrates the evolution of the probability mass function (PMF) of the model order vs record for the MVDR results, demonstrating that the number of reflectors is consistently estimated as eight or nine. Figure 2(b) focuses on the same PMFs for records 241–280. A new reflector is detected and tracked at around record 260 as also seen in Figs. 1(c) and 1(d). Significant probability is then assigned to the order of nine. The reflector becomes weaker shortly after (at around record 270) and probability is largely shifted to the order of eight. The new reflector had, in reality, appeared earlier, but was very weak and remained undetected until approximately the 260th record. As the MMPF “learns” of the reflector, significant probability for the model order shifts to a higher order as expected.

For comparison purposes, we also show here the benefit of using an MMPF vs a fixed-order PF. Figure 3 illustrates the PF layer tracking when the order is set to seven [Fig. 3(b)], eight [Fig. 3(c)], and nine [Fig. 3(d)]. Figure 3(a) shows the MVDR processor output, so that the tracking performance for a fixed order can be evaluated. When it is assumed that seven reflectors are present [Fig. 3(b)], the performance of the PF in the first states can be crucial. If the PF starts off by identifying reflectors that are not present as shown in the figure, it is possible that the algorithm will never recover with some trajectories “wandering” in the search space. The reason is that there are no “birth” or “exit” mechanisms, which are key elements of MMPFs but not simple PFs. These mechanisms enable weak or exiting directories to be removed from the estimation process and new ones to enter the search. With erroneous reflector

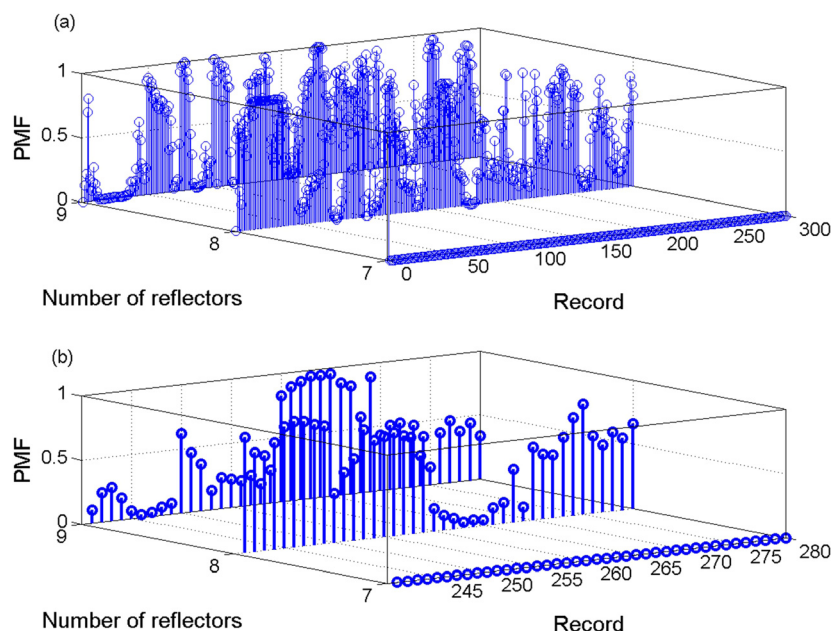


Fig. 2. (Color online) (a) PMF of the number of sedimentary reflectors for the MVDR results as calculated by the MMPF; (b) PMF of the number of sedimentary reflectors for the MVDR results for records 45–70.

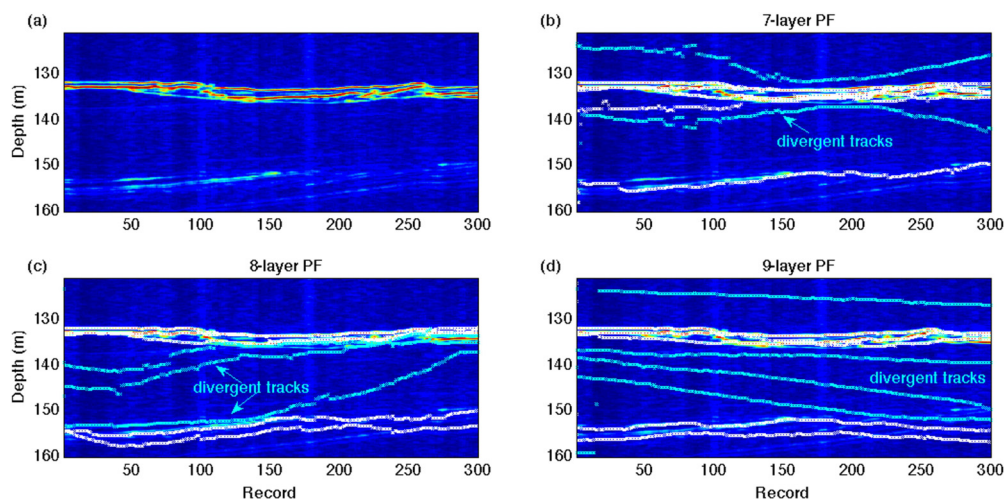


Fig. 3. (Color online) Degradation in track quality when conventional PFs are used instead of a MMPF. (a) MVDR fathometer results for Boundary 2003 data. MVDR results with classical PF MAP tracks superimposed (dots): The number of reflectors used in the PF is set to (b) seven, (c) eight, and (d) nine.

detection, several true reflectors (around 155 m in depth, for example) remain unidentified. Similarly, when an order of eight is selected, we see errors in the tracking. However, the case of missing trajectories is not as pronounced as in the previous case because of the increased order. It should be noted, here, that the true order for this problem is largely eight. When an order of nine is selected [Fig. 3(d)], the PF attempts to locate a trajectory that often does not exist. Thus in addition to the problem of the lack of an exit-birth mechanism, more errors are made because additional, non-existing tracks are forced in the estimation process. In summary, unless the order is well known, a comparison of Figs. 1 and 3 demonstrates the significant advantage of implementing an MMPF rather than a fixed-model PF.

4. Conclusions

Ocean bottom profiling from a drifting vertical array was performed using a multiple model passive fathometer particle filter. The method was demonstrated on Boundary 2003 data for tracking the evolving layer structure with an unknown number of reflectors. It is expected that sedimentary reflector tracking will facilitate geoacoustic inversion. Note that amplitudes of the reflections are also estimated by the MMPF, as mentioned in Sec. 2. These amplitudes are tightly linked to geoacoustic properties of the sediment layers and can provide a wealth of information, supplementing the sediment tracking by “localizing” reflections.

Acknowledgment

This work was supported by the Office of Naval Research, under Grant Nos. N00014-05-1-0262, N00014-09-1-0313, N00014-11-1-0320, N00014-07-1-0521, and N00014-10-1-0073.

References and links

- ¹C. H. Harrison and D. G. Simons, “Geoacoustic inversion of ambient noise: A simple method,” *J. Acoust. Soc. Am.* **112**, 1377–1389 (2002).
- ²C. H. Harrison, “Sub-bottom profiling using ocean ambient noise,” *J. Acoust. Soc. Am.* **115**(4), 1505–1515 (2004).
- ³M. Siderius, C. H. Harrison, and M. B. Porter, “A passive fathometer technique for imaging seabed layering using ambient noise,” *J. Acoust. Soc. Am.* **120**(3), 1315–1323 (2006).
- ⁴C. H. Harrison and M. Siderius, “Bottom profiling by correlating beam-steered noise sequences,” *J. Acoust. Soc. Am.* **123**(3), 1282–1296 (2008).

- ⁵P. Gerstoft, W. S. Hodgkiss, M. Siderius, C.-F. Huang, and C. H. Harrison, "Passive fathometer processing," *J. Acoust. Soc. Am.* **123**, 1297–1305 (2008).
- ⁶M. Siderius, H. Song, P. Gerstoft, W. S. Hodgkiss, P. Hursky, and C. Harrison, "Adaptive passive fathometer processing," *J. Acoust. Soc. Am.* **127**(4), 2193–2200 (2010).
- ⁷J. Gebbie, M. Siderius, L. Muzi, and J. Paddock, "Extracting the Rayleigh reflection coefficient from the passive fathometer," in *OCEANS 2010*, Seattle (Sept. 2010), pp. 1–10.
- ⁸J. Traer, P. Gerstoft, and W. S. Hodgkiss, "Ocean bottom profiling with ambient noise: A model for the passive fathometer," *J. Acoust. Soc. Am.* **129**(4), 1825–1836 (2011).
- ⁹J. V. Candy, *Bayesian Signal Processing: Classical, Modern and Particle Filtering Methods* (Wiley and Sons, Hoboken, NJ, 2009).
- ¹⁰C. Yardim, Z.-H. Michalopoulou, and P. Gerstoft, "An overview of sequential Bayesian filtering in ocean acoustics," *IEEE J. Ocean. Eng.* **36**(1), 71–89 (2011).
- ¹¹O. Carrière, J.-P. Hermand, and J. V. Candy, "Inversion for time-evolving sound-speed field in a shallow ocean by ensemble Kalman filtering," *IEEE J. Ocean. Eng.* **34**(4), 586–602 (2009).
- ¹²O. Carrière, J.-P. Hermand, J.-C. Le Gac, and M. Rixen, "Full-field tomography and Kalman tracking of the range-dependent sound speed field in a coastal water environment," *J. Mar. Syst.* **78**(4), S382–S392 (2009).
- ¹³C. Yardim, P. Gerstoft, and W. S. Hodgkiss, "Geoacoustic and source tracking using particle filtering: Experimental results," *J. Acoust. Soc. Am.* **128**(1), 75–87 (2010).
- ¹⁴J. Dettmer, S. E. Dosso, and C. W. Holland, "Sequential trans-dimensional Monte Carlo for range-dependent geoacoustic inversion," *J. Acoust. Soc. Am.* **129**(4), 1794–1806 (2011).
- ¹⁵C. Yardim, P. Gerstoft, and W. S. Hodgkiss, "Sequential geoacoustic inversion at the continental shelfbreak," *J. Acoust. Soc. Am.* In Press.
- ¹⁶I. Zorych and Z.-H. Michalopoulou, "Particle filtering for dispersion curve tracking in ocean acoustics," *J. Acoust. Soc. Am.* **124**(2), EL45–EL50 (2008).
- ¹⁷C. Yardim, P. Gerstoft, and W. S. Hodgkiss, "Tracking of geoacoustic parameters using Kalman and particle filters," *J. Acoust. Soc. Am.* **125**(2), 746–760 (2009).
- ¹⁸N. J. Gordon, D. J. Salmond, and A. F. M. Smith, "Novel approach to nonlinear/non-Gaussian Bayesian state estimation," *IEE Proc. F, Commun. Radar Signal Process.* **140**(2), 107–113 (1993).
- ¹⁹R. Jain and Z.-H. Michalopoulou, "A particle filtering approach for spatial arrival time tracking in ocean acoustics," *J. Acoust. Soc. Am.* **129**(6), EL236–EL241 (2011).
- ²⁰Z.-H. Michalopoulou and X. Ma, "Source localization in the Haro Strait primer experiment using arrival time estimation and linearization," *J. Acoust. Soc. Am.* **118**(5), 2924–2933 (2005).
- ²¹C. Andrieu and A. Doucet, "Joint Bayesian model selection and estimation of noisy sinusoids via reversible jump MCMC," *IEEE Trans. Signal Process.* **47**(10), 2667–2676 (1999).
- ²²J. R. Larocque, J. P. Reilly, and W. Ng, "Particle filters for tracking an unknown number of sources," *IEEE Trans. Signal Process.* **50**(12), 2926–2937 (2002).
- ²³B. Ristic, S. Arulampalam, and N. Gordon, *Beyond the Kalman Filter: Particle Filters for Tracking Applications* (Artech House, Boston, MA, 2004), Chaps. 1–3.